



# Tropospheric vertical column densities of NO<sub>2</sub> over managed dryland ecosystems (Xinjiang, China): MAX-DOAS measurements vs. 3-D dispersion model simulations based on laboratory-derived NO emission from soil samples

B. Mamtimin<sup>1</sup>, T. Behrendt<sup>1</sup>, M. M. Badawy<sup>1,2</sup>, T. Wagner<sup>1</sup>, Y. Qi<sup>1,3</sup>, Z. Wu<sup>1,4</sup>, and F. X. Meixner<sup>1</sup>

<sup>1</sup>Max Planck Institute for Chemistry, Mainz, Germany

<sup>2</sup>Department of Geography, Faculty of Arts, Cairo, Ain-Shams University, Egypt

<sup>3</sup>International Cooperation Department, National Center for Climate Change Strategy and International Cooperation, Beijing, China

<sup>4</sup>Institute of Geography Science, Urumqi, Xinjiang Normal University, China

Correspondence to: B. Mamtimin (buhalqem.mamtimin@mpic.de)

Received: 16 April 2014 – Published in Atmos. Chem. Phys. Discuss.: 28 July 2014

Revised: 2 December 2014 – Accepted: 16 December 2014 – Published: 23 January 2015

**Abstract.** We report on MAX-DOAS observations of NO<sub>2</sub> over an oasis–ecotone–desert ecosystem in NW China. There, local ambient NO<sub>2</sub> concentrations originate from enhanced biogenic NO emission of intensively managed soils. Our target oasis “Milan” is located at the southern edge of the Taklimakan desert, very remote and well isolated from other potential anthropogenic and biogenic NO<sub>x</sub> sources. Four observation sites for MAX-DOAS measurements were selected, at the oasis centre, downwind and upwind of the oasis, and in the desert. Biogenic NO emissions in terms of (i) soil moisture and (ii) soil temperature of Milan oasis (iii) different land-cover type sub-units (cotton, Jujube trees, cotton/Jujube mixture, desert) were quantified by laboratory incubation of corresponding soil samples. Net potential NO fluxes were up-scaled to oasis scale by areal distribution and classification of land-cover types derived from satellite images using GIS techniques. A Lagrangian dispersion model (LASAT, Lagrangian Simulation of Aerosol Transport) was used to calculate the dispersion of soil emitted NO into the atmospheric boundary layer over Milan oasis. Three-dimensional (3-D) NO concentrations (30 m horizontal resolution) have been converted to 3-D NO<sub>2</sub> concentrations, assuming photostationary state conditions. NO<sub>2</sub> column densities were simulated by suitable vertical integration of modelled 3-D NO<sub>2</sub> concentrations at those downwind and upwind locations, where the MAX-DOAS measurements were

performed. Downwind–upwind differences (a direct measure of Milan oasis’ contribution to the areal increase of ambient NO<sub>2</sub> concentration) of measured and simulated slant (as well as vertical) NO<sub>2</sub> column densities show excellent agreement. This agreement is considered as the first successful attempt to prove the validity of the chosen approach to up-scale laboratory-derived biogenic NO fluxes to ecosystem field conditions, i.e. from the spatial scale of a soil sample (cm<sup>2</sup>) to the size of an entire agricultural ecosystem (km<sup>2</sup>).

## 1 Introduction

Emissions of nitric oxide (NO) are important in regulating chemical processes of the atmosphere (Crutzen, 1987). Once emitted into the atmosphere, NO reacts rapidly with ozone (O<sub>3</sub>) to nitrogen dioxide (NO<sub>2</sub>) which, under daylight conditions, is photolysed back to NO ( $\lambda \leq 420$  nm). For that reason, NO and NO<sub>2</sub> are usually considered as NO<sub>x</sub> (NO<sub>x</sub> = NO + NO<sub>2</sub>). Ambient NO<sub>x</sub> is a key catalyst in atmospheric chemistry: during the atmospheric oxidation of hydrocarbons its ambient concentration determines whether ozone (O<sub>3</sub>) is photochemically generated or destroyed in the troposphere (Chameides et al., 1992). While the combustion of fossil fuels (power plants, vehicles) is still the most im-

portant global NO<sub>x</sub> source (approx. 25 Tg a<sup>-1</sup> in terms of mass of N), biogenic NO emissions from soils have been estimated to range between 6.6 and 9.6 Tg a<sup>-1</sup> (Denman et al., 2007). The considerable uncertainty about the range of soil biogenic NO emissions stems from widely differing estimates of the NO emission. Moreover, the uncertainties in the NO emission data from semi-arid, arid and hyper-arid regions are very large (mainly due to a very small number of measurements being available). These ecosystems, however, are considered to contribute more than half to the global soil NO source (Davidson and Kinglerlee, 1997), and make up approx. 40 % of planet Earth's total land surface (Harrison and Pearce, 2000).

Production (and consumption) of NO in the soil depends mainly on soil microbial activity and is mainly controlled by soil temperature, soil moisture and soil nutrient concentration (Conrad, 1996; Meixner and Yang 2006; Ludwig et al., 2001). Any natural or anthropogenic action that results in input of nutrients (e.g. by fertilizer application) and/or modification of soil nutrient turnover rates has a substantial effect on soil biogenic NO emission. The rapid (economically driven) intensification of arid agriculture (oasis agriculture), particularly by enlargement of the arable area and by enhancement of necessary irrigation leads inevitably to the increase of soil biogenic NO emissions. Since those microbial processes which underlay NO production and NO consumption in soils are confined to the uppermost soil layers (< 0.05 m depth, Rudolph et al., 1996), the most direct method for their characterization and quantification is usually realized by laboratory incubation of soil samples; corresponding measurements result in the determination of so-called net potential NO fluxes, which are explicit functions of soil moisture, soil temperature, and ambient NO concentration (Behrendt et al., 2014).

Tropospheric NO<sub>2</sub> column densities can be retrieved from satellite observations using differential optical absorption spectroscopy (DOAS) (e.g. Leue et al., 2001; Richter and Burrows, 2002; Beirle et al., 2004). Identification and quantification of the sources of tropospheric NO<sub>2</sub> column densities are important for monitoring air quality, for understanding radiative forcing and its impact on local climate. Ground-based Multi-Axis Differential Optical Absorption Spectroscopy (MAX-DOAS) is a novel measurement technique (Hönninger et al., 2004) that represents a significant advantage over the well-established zenith scattered sunlight DOAS instruments, which are mainly sensitive to stratospheric absorbers. From NO<sub>2</sub> slant column densities, retrieved from measurements at different elevation angles, information about tropospheric NO<sub>2</sub> profiles and/or tropospheric vertical column densities can be obtained (e.g. Sinreich et al., 2005; Wittrock et al., 2004; Wagner et al., 2011).

In this paper we concentrate (a) on ground-based MAX-DOAS measurements of slant and vertical NO<sub>2</sub> column densities over an intensively used oasis of the Taklimakan desert (NW China), (b) on biogenic NO emissions derived from lab-

oratory incubation measurements on oasis soil samples, (c) on up-scaling of the laboratory results to the oasis level, (d) calculation of atmospheric boundary layer NO<sub>2</sub> concentrations by suitable NO → NO<sub>2</sub> conversion and 3-D dispersion modelling, and (e) on simulating slant and vertical NO<sub>2</sub> column densities from the calculated 3-D-NO<sub>2</sub> distributions by integration along the MAX-DOAS light path. The final aim is comparison and discussion of the results obtained under (a) and (e).

## 2 Materials and methods

### 2.1 Research area

After two “searching field campaigns” (2008 and 2009) in the Xinjiang Uighur Autonomous Region of NW China, the oasis “Milan” has been identified as the target oasis for the presented research. The contemporary oasis Milan, identical to the ancient Silk Road post “Miran”, belongs to the county “Ruoqiang” of the Xinjiang province and is located in the southern Taklimakan Desert on the foot of the Altyn-Tagh Mountains (39.25° N, 88.92° E, 998 m a.s.l.). In the early 1950s, the delta-shaped oasis (see Fig. 1) was established as an agricultural co-operative “state farm” (*Xinjiang Production and Construction Crop*) and covers nowadays about 100 km<sup>2</sup>. Milan oasis can be geomorphologically classified as a “mountain–oasis–ecotone–desert system (MOED system)” consisting of Gobi (gravel) desert, a salty transition zone surrounding the oasis, and dryland farming with irrigation. The latter consists only of two crops, cotton and jujube trees (*Ziziphus Jujuba* L., “red date”), which are planted, irrigated and fertilized following standardized protocols and growing on rectangular fields (approx. 10 ha) of pure cultures or mixtures of it. The general energy supply of Milan oasis is entirely provided by nearby hydropower plants, and battery-powered trikes dominate the local public and private transport. Consequently, anthropogenic NO<sub>x</sub> emissions of Milan oasis are considered as very low, if not negligible. Beyond that, Milan oasis is isolated by the desert from neighbouring oases by 80 to 400 km. Therefore, the dominant NO<sub>x</sub> source of Milan oasis are biogenic NO emissions from its intensively managed crop fields; the oasis can be undoubtedly considered as a large “hotspot in the middle of nothing”. Given this very specific situation, it is certainly justified to assume that (a) NO<sub>2</sub> concentrations in the atmospheric boundary layer over Milan oasis are only caused by the oasis itself, and (b) free tropospheric NO<sub>2</sub> concentrations, which are usually due to large-scale tropospheric NO<sub>2</sub> advection, are negligible.

According to the Köppen classification (Köppen, 1931; Kottke et al., 2006), Milan oasis owns a cold desert climate (BWk), which is dominated by long hot summers (30 years' mean: 29 °C) and cold winters (30 years' mean: -6 °C). Mean annual precipitation amounts 28.5 mm, mean annual

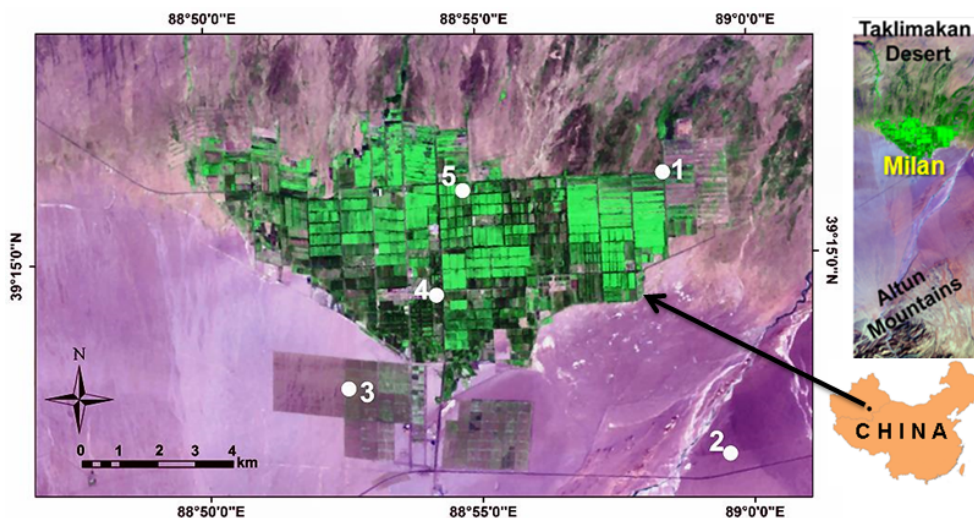


**Figure 1.** Satellite map (Landsat ETM+; 2011) of Milan oasis, Xinjiang, NW China (The map has an area of 338 km<sup>2</sup>). The white circles show the sites of in situ measurements: natural forest (1), desert (2), jujube (3), hotel/oasis station (4) and cotton field (5).

evaporating capacity is 2920 mm, mean wind direction is NE to E, and mean wind speed is 2.7 m s<sup>-1</sup>.

## 2.2 In situ measurements

A field campaign was performed at Milan oasis, from 24 May to 26 June, 2011. A total of 32 individual MAX-DOAS measurements (approx. 20 min) were performed by two Mini-MAX-DOAS instruments (partially simultaneously) on 21 days during the 2011 campaign at the NE natural forest site (1), desert site (2), jujube site (3) and hotel station in Milan oasis centre (4). Accompanying data of wind direction, wind speed, air temperature, barometric pressure, global and net radiation were observed at sites (1)–(5) at 1.8 m above ground (at NE natural forest: 11 m; at hotel station: 23 m). Soil temperature (at 0.05 m depth) as well as rainfall (amount and intensity) were recorded at all sites in 2011.

### 2.2.1 Ground-based measurements of vertical column densities of NO<sub>2</sub>

MAX-DOAS observes scattered sunlight under various (mostly slant) elevation angles. From combinations of the retrieved NO<sub>2</sub> slant column densities (SCDs) obtained at different elevation angles, information on the vertical NO<sub>2</sub> profile and/or on the corresponding vertical column density (VCD) can be obtained (e.g. Hönninger et al., 2002; Sinreich et al., 2005; Wittrock et al., 2004; Wagner et al., 2011). Spectral calibration of the MAX-DOAS instruments was performed by fitting a measured spectrum to a convoluted solar spectrum based on a high-resolution solar spectrum (Kurucz et al., 1984). Several trace gas absorption cross-sections of NO<sub>2</sub> at 294 K (Vandaele et al., 1996), H<sub>2</sub>O at 290 K (Rothman et al., 2005), Glyoxal at 296 K (Volkamer et al., 2005),

O<sub>3</sub> at 243 K (Bogumil et al., 2003) and O<sub>4</sub> at 286 K (Hermans et al., 1999) were convolved to match the resolution of the instrument and then used in the spectral analysis using a wavelength range of 420–450 nm (also a Ring spectrum was included in the fitting process). The output of the spectral analysis is the NO<sub>2</sub> SCD, which represents the NO<sub>2</sub> concentration integrated along the corresponding light paths through the atmosphere.

Since a spectrum measured in the zenith direction (a so-called Fraunhofer reference spectrum) is included in the fit process to remove the strong Fraunhofer lines, the retrieved NO<sub>2</sub> SCD actually represents the difference between the SCDs of the measurement and the Fraunhofer reference spectrum; it is usually referred to as differential SCD or DSCD<sub>meas</sub>. The tropospheric DSCD for the elevation angle  $\alpha$  can be derived from MAX-DOAS observation by subtracting the NO<sub>2</sub> DSCD for the closest zenith observation  $\alpha_0 = 90^\circ$ :

$$\text{DSCD}_{\text{trop}}(\alpha) = \text{DSCD}_{\text{meas}}(\alpha) - \text{DSCD}_{\text{meas}}(\alpha_0). \quad (1)$$

DSCDs are converted into VCDs (the vertically integrated concentration) using so-called air mass factors (AMFs, Solomon et al., 1987), defined by

$$\text{AMF} = \text{SCD}/\text{VCD}. \quad (2)$$

In many cases AMFs are determined from radiative transfer simulations (Solomon et al., 1987). However, if trace gas column densities are retrieved from MAX-DOAS observations at high elevation angles ( $> 10^\circ$ ), the AMF can be determined by the so-called geometric approximation (Hönninger et al., 2002; Brinksma et al., 2008; Wagner et al., 2010):

$$\text{AMF}_{\text{trop}} \approx \frac{1}{\sin(\alpha)}. \quad (3)$$

In this study, the tropospheric vertical column density ( $VCD_{\text{trop}}$ ) is obtained from  $DSCD_{\text{trop}}(\alpha)$  as discussed by Wagner et al. (2010):

$$VCD_{\text{trop}} = \frac{DSCD_{\text{trop}}(\alpha)}{AMF_{\text{trop}}(\alpha - AMF_{\text{trop}}(\alpha_0))}. \quad (4)$$

During the field experiments, the MAX-DOAS instruments have been mounted on solid tables (aluminium structure) at approx. 11 m a.g.l. (NW natural forest, hotel station) and 3.5 m a.gr. (remainder of sites) with the telescope facing northwards. Observations were always made on elevation angles of 0°, 2°, 4°, 6°, 8°, 10°, 15°, 20°, 45° and 90°. The  $VCD_{\text{trop}}$  were determined from measurements at 15°. The potential importance of scattering on the interpretation of the MAX-DOAS measurements depends on two main aspects: first on the height of the trace gas layer and second on the amount of aerosols. In our case the trace gas layer is shallow and the aerosol amount is low (see Sect. 2.2.8). Thus scattering effects can be neglected. However, for comparison of the  $DSCD_{\text{trop}}$  data obtained by MAX-DOAS with the simulated SCDs obtained from 3-D distributions of NO<sub>2</sub> concentration – calculated with LASAT (Lagrangian Simulation of Aerosol Transport) – on the basis of laboratory-derived net potential NO<sub>2</sub> fluxes) the lower elevation angles (2°, 4°) for  $DSCD_{\text{trop}}(\alpha)$  have been used, which have a much higher sensitivity to the observed NO<sub>2</sub>.

For classifying all MAX-DOAS measurements whether they were made upwind, downwind, or in the centre of Milan oasis, their observation position was related to the mean wind direction during each measurement period. Wind measurements were part of accompanying in situ measurements (see below).

### 2.2.2 Accompanying measurements

Wind direction, wind speed, air temperature, relative humidity, barometric pressure and rainfall intensity were measured by combined weather sensors (weather transmitter WXT510, Vaisala, Finland). All five weather sensors were operated side-by-side for 1 week before being mounted at the individual measurement sites (1)–(5). Based on these results, all meteorological data measured between 3–24 July 2011 were corrected using one of the sensors as reference. All combined weather sensors' data, as well as those of net radiation (four-component net radiation sensor, model NR01, Hukseflux, the Netherlands) and soil temperature (thermistor probe, model 109, Campbell Scientific, USA) were recorded every minute. Ambient O<sub>3</sub> concentrations and NO<sub>2</sub> photolysis rates were also measured in situ; both quantities are necessary to calculate the NO → NO<sub>2</sub> conversion factor (see Sect. 2.2.8). Ozone concentrations were measured by UV-absorption spectroscopy (model 49i, ThermoFisher Scientific, USA) and NO<sub>2</sub> photolysis rate by a filter radiometer (model 2-Pi-JNO<sub>2</sub>, Metcon, Germany) at 1 min intervals.

### 2.2.3 Soil samples

Microbial processes responsible for biogenic NO emission are confined to the uppermost soil layers (Galbally and Johansson, 1989; Rudolph et al., 1996; Rudolph and Conrad, 1996). Consequently, composite soil samples (1 kg of top soil, 0–5 cm depth) were collected at the individual sites of Milan oasis (natural forest, cotton, jujube, cotton and jujube mixture, desert). All samples (air dried) were sent from Xinjiang to Germany by air cargo and stored refrigerated (+4 °C) prior to laboratory analysis of the net potential NO flux (see below). Sub-samples were analysed for dry bulk soil density (ISO 11272), pH (ISO 10390), electrical conductivity (salinity, ISO 11265), contents of nitrate and ammonium (ISO 14256), total carbon and total nitrogen (ISO 10649 and ISO 13878), texture (ISO 11277), as well as the soil water potential (pF values 1.8, 2.5, 4.2, Hartge and Horn, 2009).

Electrical conductivity varied between 1.6 and 9.5 dS m<sup>-1</sup> within the managed soils, and was 59.8 and 3.0 dS m<sup>-1</sup> in the natural forest and desert soils, respectively. Commercially available soil moisture probes – e.g. TDR (Time Domain Reflectometry) and FDR (Frequency Domain Reflectometry) – show extreme interferences for soils of > 2 dS m<sup>-1</sup> (see Kargas et al., 2013) and their calibration for such soils is extremely challenging, if possible at all. Indeed, FDR signals monitored in Milan oasis' soils were extremely noisy and spurious. Nevertheless, up-scaling of the laboratory-derived net potential NO fluxes needs data of the uppermost layer of each soil of Milan oasis land types (see Sect. 2.2.6). For that, as the most reasonable approximation, it was decided to use the individual (constant) gravimetric soil moisture content which corresponds to the so-called “wilting point”. The latter was determined by laboratory water tension measurements (pF 4.2) on undisturbed soil cores from each land-cover type. The wilting point is defined as that soil moisture in the root zone which would cause irreversible wilting of plants. Wilting point conditions in the uppermost soil layers (2 cm) of soils in the Taklimakan Desert are easily reached, since evaporation is extremely high (evaporating capacity 2920 mm<sup>-1</sup>). Even after flooding irrigation of Milan oasis' crop fields, these conditions have repeatedly been observed within at least 3 days by visual inspections.

### 2.2.4 Laboratory determination of net potential NO fluxes

The methodology for the laboratory measurement of the NO flux from soil was developed at the end of the 1990s (Yang and Meixner, 1997) and has been continuously used during the last two decades (Otter et al., 1999; Kirkman et al., 2001; van Dijk and Meixner, 2001; Feig et al., 2008a; Feig et al., 2008b, 2009; Yu et al., 2008, 2010a, b; Ashuri, 2009; Gelfand et al., 2009; Bargsten et al., 2010). The methodology has been significantly improved in the frame of this study and is described in detail by Behrendt et al. (2014).

Generally, the release of gaseous NO from soil is the result of microbial NO production and simultaneous NO consumption. The latter is, as shown by Behrendt et al. (2014), particularly for arid and hyper-arid soils, negligible. Applying the laboratory dynamic chamber method, the release of NO is determined by incubating aliquots of the soil samples in a dynamic chamber system under varying, but prescribed conditions of soil moisture, soil temperature and chamber's headspace NO concentrations. From the difference of measured NO concentrations at the outlets of each soil-containing chamber and an empty reference chamber, actual net potential NO fluxes (in terms of mass of nitric oxide per area and time) is calculated as function of soil moisture and soil temperature. For that, a known mass (approx. 60 g dry weight) of sieved (2 mm) and wetted (to water holding capacity) soil is placed in one of six Plexiglas chambers (volume  $9.7 \times 10^{-4} \text{ m}^3$ ) in a thermo-controlled cabinet (0–40 °C). After passing through a purification system (PAG 003, Ecophysics, Switzerland), dry pressurized, zero (i.e. "NO-free") air is supplied to each chamber, controlled by a mass flow controller ( $4.167 \times 10^{-5} \text{ m}^3 \text{ s}^{-1}$ ). The outlet of each chamber is connected via a switching valve system to the gas-phase chemiluminescence NO analyser (model 42i-TL, Thermo Fisher Scientific Inc., USA) and to the non-dispersive infrared CO<sub>2</sub>/H<sub>2</sub>O analyser (model LICOR 840A, LI-COR Biosciences Inc., USA). During a period of 24–48 h, the soil samples are slowly drying out, hence providing the desired variation over the entire range of soil moisture (i.e. from water-holding capacity to wilting point conditions and completely dry soil). During the drying-out period, the temperature of thermo-controlled cabinet is repeatedly changed from 20 to 30 °C, hence providing the desired soil temperature variation (Behrendt et al. 2014). Occasionally, nitric oxide standard gas (200 ppm) is diluted into the air purification system via a mass flow controller; this allows the control of the chamber headspace NO concentration when determining NO consumption rate of the soil sample. The actual soil moisture content of each soil sample is determined by considering the H<sub>2</sub>O mass balance of each chamber, where the temporal change of the chamber's headspace H<sub>2</sub>O concentration is explicitly related to the evaporation rate of the soil sample. Tracking the chamber's headspace H<sub>2</sub>O concentration throughout the drying-out period and relating it to the gravimetrically determined total soil mass at the start and end of the measurement period delivers the actual gravimetric soil moisture content of the soil sample (Behrendt et al., 2014).

As shown during the last two decades (Yang and Meixner, 1997; Otter et al., 1999; Kirkman et al., 2001; van Dijk and Meixner, 2001; van Dijk et al., 2002; Meixner and Yang, 2006; Yu et al., 2008, 2010; Feig et al., 2008; Ashuri, 2009; Feig, 2009; Gelfand et al., 2009 and Bargsten et al., 2010), the dependence of NO release from gravimetric soil moisture and soil temperature can be characterized by two explicit dimensionless functions, the so-called optimum soil mois-

ture curve  $g(\theta_g)$  and the exponential soil temperature curve  $h(T_{\text{soil}})$ :

$$g(\theta_g) = \left(\frac{\theta_g}{\theta_{g,0}}\right)^a \exp\left[-a\left(\frac{\theta_g}{\theta_{g,0}} - 1\right)\right] \quad (5)$$

$$h(T_{\text{soil}}) = \exp\left[\frac{\ln Q_{10,\text{NO}}}{10}(T_{\text{soil}} - T_{\text{soil},0})\right], \quad (6)$$

where  $\theta_g$  is the dimensionless gravimetric soil moisture content,  $\theta_{g,0}$  the so-called optimum gravimetric soil moisture content (i.e. where the maximum NO release has been observed),  $a$  is the soil moisture curve's shape factor (solely derived from NO release and gravimetric soil moisture data which have been observed during the drying-out measurements, see Behrendt et al. 2014),  $T_{\text{soil}}$  is the soil temperature (in °C),  $T_{\text{soil},0}$  is the reference temperature (here: 20 °C) and  $Q_{10,\text{NO}}$  is the (logarithmic) slope of  $h(T_{\text{soil}})$ , defined by

$$Q_{10,\text{NO}} = \frac{\ln F_{\text{NO}}(\theta_{g,0}, T_{\text{soil},1}) - \ln F_{\text{NO}}(\theta_{g,0}, T_{\text{soil},0})}{T_{\text{soil},1} - T_{\text{soil},0}}, \quad (7)$$

where  $T_{\text{soil},1}$  is a soil temperature which is 10 K different from  $T_{\text{soil},0}$  (here: 30 °C). The actual NO fluxes  $F_{\text{NO}}$  ( $\text{ng m}^{-2} \text{ s}^{-1}$ ; in terms of mass of nitric oxide) are defined by

$$F_{\text{NO}}(\theta_{g,0}, T_{\text{soil},0}) = \quad (8)$$

$$\frac{Q}{A_{\text{soil}}}[m_{\text{NO},\text{cham}}(\theta_{g,0}, T_{\text{soil},0}) - m_{\text{NO},\text{ref}}] f_{C,\text{NO}}$$

$$F_{\text{NO}}(\theta_{g,0}, T_{\text{soil},1}) = \quad (9)$$

$$\frac{Q}{A_{\text{soil}}}[m_{\text{NO},\text{cham}}(\theta_{g,0}, T_{\text{soil},1}) - m_{\text{NO},\text{ref}}] f_{C,\text{NO}},$$

where  $Q$  is the purging rate of the dynamic chambers ( $\text{m}^3 \text{ s}^{-1}$ ),  $A_{\text{soil}}$  is the cross-section of the dynamic chamber ( $\text{m}^2$ ) and  $m_{\text{NO},\text{cham}}$  and  $m_{\text{NO},\text{ref}}$  are the NO mixing ratios (ppb) observed under conditions  $(\theta_{g,0}, T_{\text{soil},0})$  and  $(\theta_{g,0}, T_{\text{soil},1})$  at the outlets of each soil chamber and the reference chamber, respectively. The conversion of NO mixing ratios to corresponding NO concentrations ( $\text{ng m}^{-3}$ , in terms of mass of nitric oxide) is considered by  $f_{C,\text{NO}}$  ( $= 572.5 \text{ ng m}^{-3} \text{ ppb}^{-1}$  under STP conditions). Finally, the net potential NO flux,  $F_{\text{NO}}(\theta_g, T_{\text{soil}})$  is given by

$$F_{\text{NO}}(\theta_g, T_{\text{soil}}) = F_{\text{NO}}(\theta_{g,0}, T_{\text{soil},0}) g(\theta_g) h(T_{\text{soil}}). \quad (10)$$

This net potential NO flux is specific for each soil sample, hence for sites (1), (2), (4) and (5) of Milan oasis; the actual NO flux of the sites is calculated by applying corresponding field data of gravimetric soil moisture and soil temperature. This procedure has been successfully applied for a variety of terrestrial ecosystems (e.g. Otter et al., 1999; van Dijk et al., 2002; Ganzeveld et al., 2008). For soils of the Zimbabwean Kalahari (Ludwig et al., 2001; Meixner and Yang, 2006), for a German grassland soil (Mayer et al., 2011), but also for

Brazilian rainforest soils (van Dijk et al., 2002), soil biogenic NO fluxes derived from the described laboratory incubation method have been successfully verified by field measurements using both field dynamic chamber and micrometeorological (aerodynamic gradient) techniques.

### 2.2.5 Classification and actual distribution of Milan fields

Image classification is likely to assemble groups of identical pixels found in remotely sensed data into classes that match the informational categories of user interest by comparing pixels to one another and to those of known identity. For the purposes of our study, land-cover classification was carried out based on two Quickbird images (0.6 m ground resolution, DigitalGlobe, <http://www.digitalglobe.com>) acquired on 09 April and 31 August 2007 respectively, with the aid of a recent ETM+ Landsat image (141/033, <http://earthexplorer.usgs.gov/>) acquired on 25 April 2011 (15 and 30 m spatial resolution). A major advantage of using Quickbird images of high spatial resolution images is that such data greatly reduce the mixed-pixel problem (a “mixed pixel” consists of several land-cover classes) and provide a greater potential to extract much more detailed information on land-cover structures (e.g. field borders, buildings, roads) than medium or coarse spatial resolution data, whether using on-screen digitizing or image classification.

However, we take advantage of resolution merge processing to increase the spatial resolution of the Landsat image from 30 to 15 m for the bands 1–5 and 7 for better land-cover mapping and to update the land-cover map from 2007 to 2011. Then, we defined different areas of interest (AOIs) to represent the major land covers with the aid of in situ GPS data collection (45 points). Next, we increased the number of AOIs based on the image spectral analysis method. After that, supervised classification was performed using the maximum likelihood parametric rule and probabilities. This classifier uses the training data by means of estimating means and variances of the classes, which are used to estimate Bayesian probability and also consider the variability of brightness values in each class. For that, it is the most powerful classification method when accurate training data are provided, and is one of the most widely used algorithms (Perumal and Bhaskaran, 2010). As a result, five major ecosystems were determined: cotton, jujube, cotton/jujube mixture fields, desert and plant cover. The cotton and the jujube fields are the most dominant types. Finally, the classified land-cover image was converted into vector format using polygon vector data type to be implemented in LASAT analysis as sources of NO flux and for the purpose of estimating NO concentrations. The map includes 2500 polygons of different sizes as sub-units of Milan major land cover.

### 2.2.6 Two-dimensional distribution of soil NO emissions of Milan oasis

The soil NO emission sources of Milan oasis were defined by individual source units, which have been identified as those sub-units (polygons) of the land-cover vector map consisting of natural forest or desert, or covered by cotton, jujube, cotton/jujube mixture. Two identifiers have been attributed to each source unit: (a) a metric coordinate whose numerical format refers to the corner of the corresponding polygon, and (b) a unique ID number followed by a description of its land-cover type. The soil NO source strength (i.e. actual NO flux, see Sect. 2.2.4) of each source unit has been calculated from the corresponding net potential NO flux, the land-cover type specific gravimetric soil moisture content (“wilting point”) and the actual soil temperature, which has been in situ measured for each of the land-cover type of Milan oasis (see Sect. 2.2.2). Those polygons not matching the mentioned land-cover types and other tiny polygons generated by digital image processing techniques were dismissed to avoid intricate geometric errors affecting NO emission data. In other words, these “other classes” were dissolved before performing LASAT analysis to avoid extreme values.

### 2.2.7 Three-dimensional distribution of NO concentrations by Lagrangian dispersion modelling

Having the actual NO source units of the Milan oasis available, the 3-D distribution of NO concentrations in the atmospheric boundary layer (0–1500 m a.g.r.) over Milan oasis have been calculated by the Lagrangian dispersion model LASAT (German VDI Guidelines VDI3945, part 3; see Janicke Consulting, 2011). LASAT is a state-of-the-art model, since (a) LASAT is one of those transport dispersion models of air pollution which is officially licensed for legal use of environmental issues (in Germany), and (b) among comparable micro-scale (e.g. street canyons) transport-dispersion models LASAT considers at least chemical transformations of first order and still remains truly operational. Being a transport dispersion model, LASAT basically considers advection (“pixel cross-talk”) by applying the 3-D continuity equation for any chosen tracer (see German VDI Guidelines VDI3945, part 3, see Janicke Consulting, 2011). For that, pre-processing of meteorological parameters (i.e. 3-D wind distributions, based on meteorological in situ measurements, see Sect. 2.2.2) and calculation of dispersion parameters ( $\sigma_y$ ,  $\sigma_z$ ) have to be performed. Unfortunately, it was difficult to obtain fine resolution using LASAT individually. Therefore, the LASAT model was integrated with the Geographic Information System (ArcGIS) by using an advanced module, namely LASarc (IVU Umwelt GmbH, 2012). LASarc allowed us to calculate NO concentrations using relatively fine resolution of 30 m × 30 m and taking advantage of using the integrated map colour scheme in ArcGIS. This module has

been used to realize Milan oasis' complex NO source configuration and to set up calculations of LASAT.

The model was designed to calculate NO concentrations at 16 different vertical layers (0–3, 3–5, 5–10, 10–20, 20–30, 30–50, 50–70, 70–100, 100–150, 150–200, 200–300, 300–400, 400–500, 500–700, 700–1000 and 1000–1500 m a.gr.). The horizontal resolution is 30 m, in both the *x*-direction (W–E) and the *y*-direction (S–N), which results in 656 (*x*) and 381 (*y*) grids for the Milan oasis domain. LASAT's meteorological input data contain a variety of parameters, namely start and end time (*T*<sub>1</sub>, *T*<sub>2</sub>), wind speed (*U*<sub>a</sub>) and wind direction (*R*<sub>a</sub>) at anemometer height (*H*<sub>a</sub>), average surface roughness (*Z*<sub>0</sub>), and atmospheric stability (in terms of stability classes). These parameters have been provided in a time-dependent tabular form, updated every 30 minutes (except *Z*<sub>0</sub>). Average (30 min) wind speed and wind direction data have been calculated from in situ measurements (1 min resolution, see Sect. 2.2.2).

LASAT's pre-processing module determines the vertical profile of wind speed according to the well-known logarithmic relation

$$U(z) = \frac{u_*}{k} \ln\left(\frac{z}{Z_0}\right), \quad (11)$$

where *U*(*z*) is the horizontal wind speed (m s<sup>-1</sup>) at height *z*(m), *u*<sub>\*</sub> is the friction velocity (m s<sup>-1</sup>), *k* is the dimensionless von Karman constant (= 0.4, Simiu and Scanlan, 1996) and *Z*<sub>0</sub> is the surface roughness length (m). LASAT's pre-processing module accepts only one individual value for *Z*<sub>0</sub>; nevertheless, the required mean value has been calculated from all of *Z*<sub>0</sub> of Milan oasis domain, which have been assigned to each of the sub-units (polygons) of the vector land-cover map (see Sect. 2.2.5). For individual *Z*<sub>0</sub>, we calculated land-cover specific NDVI data (normalized differential vegetation index) from Landsat ETM+ image (141/033):

$$\text{NDVI} = \frac{r_{\text{NIR}} - r_{\text{RED}}}{r_{\text{NIR}} + r_{\text{RED}}}, \quad (12)$$

where NIR is the reflectance in the near-infrared bandwidth (0.77–0.90 μm) and RED is the reflectance in the red bandwidth (0.63–0.69 μm). In Landsat ETM+ images, these correspond to bands 4 and 3, respectively. Finally, *r*<sub>NIR</sub> and *r*<sub>RED</sub> are the corresponding ratios of reflected and incident energy as a function of wavelength (see Chander and Markham, 2003). Then, surface roughness grid data were estimated as

$$Z_0(x, y) = \exp(a_{xy} \text{NDVI}(x, y) + b_{xy}), \quad (13)$$

where *a*<sub>xy</sub> and *b*<sub>xy</sub> are constants, which are, according to Morse et al. (2000), derived from NDVI(*x*, *y*) and GPS(*x*, *y*) data for known sample pixels representing the earlier classified land-cover types, namely natural forest, desert, cotton, jujube, and cotton/jujube mixture. Corresponding land-cover type *Z*<sub>0</sub> are 0.45, 0.01, 0.18, 0.26 and 0.22 m, respectively;

the required average value over the entire LASAT model domain results in *Z*<sub>0</sub> = 0.22 ± 0.158 m.

Besides mechanical turbulence (*Z*<sub>0</sub>), atmospheric stability most affects the dispersion of trace substances. For Milan oasis' atmospheric boundary layer, atmospheric stability has been calculated according to the "solar radiation/delta T (SRDT)" method in 30 min intervals. This method (see Turner, 1994) is widely accepted because of its simplicity and its representativeness for atmospheric stability over open country and rural areas, like the Milan oasis domain. Daytime stability classes are calculated from in situ measurements of solar radiation and horizontal wind speed (see Sect. 2.2.2).

Finally, 30 min means of all parameters and input variables of LASAT have been calculated. Using these, about 4 × 10<sup>6</sup> gridded data points of 3-D NO concentration have been calculated for each time period considered in Sect. 3.2.

### 2.2.8 Simulation of SCD<sub>NO<sub>2</sub></sub> and VCD<sub>NO<sub>2</sub></sub> by spatial integration of LASAT results

There is only one tool to provide a robust relationship between biogenic soil NO emissions on the one hand and MAX-DOAS observed SCDs and VCDs on the other hand: the exact simulation of the MAX-DOAS measurement through spatial integration of 3-D NO concentrations calculated by LASAT (followed by NO→NO<sub>2</sub> conversion). At a given location of the MAX-DOAS measurement, integration must be performed from the height where the MAX-DOAS instrument has been set up (*h*<sub>MAX-DOAS</sub>) to the end of the atmospheric boundary layer (*h*<sub>ABL</sub> = 1500 m a.gr.) along two virtual light paths: (a) the vertical-up path (VCD) and (b) the slant path (SCD), according to the selected elevation angle of each MAX-DOAS measurement.

Calculation of simulated VCD for NO (VCD<sub>NO,sim</sub>) at the location of a MAX-DOAS instrument is achieved as follows: (a) determination of the NO mass density (ng m<sup>-2</sup>) of the vertical column between *h*<sub>MAX-DOAS</sub> and *h*<sub>ABL</sub>; this is obtained by adding NO concentrations (ng m<sup>-3</sup> in terms of mass of nitric oxide) of all LASAT cells in the vertical direction over that 30 m × 30 m grid, which contains the location of the MAX-DOAS instrument, multiplied by the height difference Δ*h* = *h*<sub>ABL</sub> – *h*<sub>MAX-DOAS</sub> (in m), (b) multiplying that NO mass density by the ratio of Avogadro's number (6.02217 × 10<sup>26</sup> molecules kmol<sup>-1</sup>) and the molecular weight of NO (30.0061 × 10<sup>12</sup> ng kmol<sup>-1</sup>) delivers the desired value of SCD<sub>NO,sim</sub> in units of molecules m<sup>-2</sup> (× 10<sup>-4</sup>: molecules cm<sup>-2</sup>) at the location of the MAX-DOAS instrument. Calculation of simulated SCD for NO (SCD<sub>NO,sim</sub>) requires the determination of the 3-D light path through the trace gas layer. Positioning of MAX-DOAS's telescope was always to the north; the selected MAX-DOAS elevation angle α and *h*<sub>ABL</sub> deliver the length of the slant light path (= *h*<sub>ABL</sub>/sin α). The desired SCD<sub>NO,sim</sub> (in molecules m<sup>-2</sup>) results from the NO mass density of the slant column mul-

multiplied by the length of the slant light path, where the NO mass density is equivalent to the sum of all NO concentrations of those LASAT cells which are intersected by the slant light path from the position of the MAX-DOAS instrument to  $h_{\text{ABL}}$ .

For conversion of  $\text{VCD}_{\text{NO},\text{sim}}$  to  $\text{VCD}_{\text{NO}_2,\text{sim}}$  and  $\text{SCD}_{\text{NO},\text{sim}}$  to  $\text{SCD}_{\text{NO}_2,\text{sim}}$  it is assumed that the photostationary state (PSS) of the triad NO, NO<sub>2</sub> and O<sub>3</sub> is established in Milan oasis' atmospheric boundary layer. According to Leighton (1961) this chemical equilibrium state is due to fast photochemical reactions, namely  $\text{NO} + \text{O}_3 \rightarrow \text{NO}_2 + \text{O}_2$  and  $\text{NO}_2 + h\nu \rightarrow \text{NO} + \text{O}$ , from which the so-called photostationary state NO<sub>2</sub> concentration ( $\text{NO}_{2,\text{PSS}}$ ) can be derived as

$$[\text{NO}_{2,\text{PSS}}] = \frac{[\text{O}_3][\text{NO}]k_1}{j(\text{NO}_2)}, \quad (14)$$

where  $[\text{O}_3]$  is the ozone number density (molecules  $\text{cm}^{-3}$ ; calculated from in situ measured O<sub>3</sub> concentrations, see Sect. 2.2.2),  $[\text{NO}]$  is the NO number density,  $k_1$  is the reaction coefficient of the  $\text{NO} + \text{O}_3 \rightarrow \text{NO}_2 + \text{O}_2$  reaction ( $\text{cm}^3 \text{ molecules}^{-1} \text{ s}^{-1}$ ; Atkinson et al., 2004), and  $j(\text{NO}_2)$  is the in situ measured NO<sub>2</sub> photolysis rate (in  $\text{s}^{-1}$ ; see Sect. 2.2.2). Finally,  $\text{VCD}_{\text{NO}_2,\text{sim}}$  and  $\text{SCD}_{\text{NO}_2,\text{sim}}$  are calculated from  $\text{VCD}_{\text{NO},\text{sim}}$  and  $\text{SCD}_{\text{NO},\text{sim}}$  by

$$\begin{aligned} \text{VCD}_{\text{NO}_2,\text{sim}} &= \text{CF}_0 \times \text{VCD}_{\text{NO},\text{sim}} \text{ and } \text{SCD}_{\text{NO}_2,\text{sim}} \\ &= \text{CF}_0 \times \text{SCD}_{\text{NO},\text{sim}}, \end{aligned} \quad (15)$$

where the  $\text{NO} \rightarrow \text{NO}_2$  conversion factor is defined by  $\text{CF}_0 = [\text{O}_3]k_1/j(\text{NO}_2)$ .

Since the  $\text{NO}-\text{NO}_2-\text{O}_3$  photochemical equilibrium could not be handled by LASAT's "chemical" algorithm, we decided to use measured data (O<sub>3</sub> mixing ratio, NO<sub>2</sub> photolysis rate, see Sect. 2.2.2) to convert the calculated 3-D NO mixing ratio to the photo-stationary 3-D NO<sub>2</sub> mixing ratio. For that, a constant vertical O<sub>3</sub> mixing ratio (up to 1500 m a.gr.) is assumed over Milan oasis. This is justified by the fact that, particularly in arid and hyper-arid landscapes at midday conditions (maximum of insolation), the entire atmospheric boundary layer is intensively mixed, which is due to extensive convective heating of the surface by the sun which produces powerful buoyant thermals that establish the so-called mixing layer. Consequently, a uniform vertical mixing ratio is expected for trace gases with chemical lifetimes greater than the exchange time of the atmospheric boundary layer (see Husar et al. 1978; Stull, 1988). This assumption is valid for ozone. Vertically constant O<sub>3</sub> mixing ratio has been reported for the atmospheric boundary layer over semi-arid southern Africa (Meixner et al., 1993). Concerning the vertical distribution of  $j(\text{NO}_2)$ , it is obvious that the downward component of the actinic flux increases with increasing elevation due to the decreasing optical thickness of the scattering air masses. However, the altitude effect on the actinic flux in the first kilometre of the troposphere is typically very

small. Trebs et al. (2009) used the Tropospheric Ultraviolet Visible model to calculate the typical vertical change of the actinic flux and found a vertical gradient of 1.1 %  $\text{km}^{-1}$ . Consequently, our calculations of the NO to NO<sub>2</sub> conversion in the boundary layer over Milan oasis (1500 m a.gr.) have not considered any potential vertical change of the  $j(\text{NO}_2)$  values measured at ground level. Nevertheless, for the case of our measurements the locally enhanced NO values caused by the soil emissions have a small but systematic effect on the ozone concentration, and thus also on the Leighton ratio: close to the surface (below about 50 m) the NO concentrations can be quite large, with maximum values up to about 10 ppb. Consequently, the ozone concentration will be reduced due to the reaction with NO by up to about 10 ppb. This means that the Leighton ratio will be reduced by up to about 25 %. Although the reduction of the ozone mixing ratio will be partly compensated by mixing with air from higher altitudes, the simulated NO<sub>2</sub> mixing ratios might overestimate the true NO<sub>2</sub> mixing ratios by up to about 25 %. Probably the true overestimation for our measurements is much smaller because the typical NO mixing ratio within the lowest 100 m is much lower than 10 ppb.

### 3 Results and discussion

#### 3.1 Land-cover type specific net potential NO fluxes

Net potential NO fluxes (as functions of soil temperature and moisture) have been determined by incubation of samples which have been taken from the top-soil of Milan oasis' major land-cover types, i.e. natural forest, desert, cotton, jujube and cotton/jujube mixture (see Sect. 2.2.4). Figure 2 shows the laboratory-derived net potential NO flux ( $F_{\text{NO}}$ ) from soils of the most contrasting land-cover types of Milan oasis (irrigated and fertilized fields of cotton, jujube, cotton/jujube mixture and desert).

Net potential NO fluxes of the natural forest land-cover type are not shown, because laboratory incubation measurements have shown that there is no significant NO release from these soils, most likely due to its high electrical conductivity (salt content). Optimum gravimetric soil water contents (i.e. where the maximum of  $F_{\text{NO}}$  is observed) for desert, managed cotton and managed jujube soils have one thing in common – very low values of  $\theta_{\text{g,opt}}$  (0.009–0.017) for soil temperatures of 50 °C. During the vegetation period (April–September), soil temperatures of >40 °C are easily reached for the soils of Milan oasis, particularly for the desert soils. While the nature of all Milan oasis' soils is arid/hyper-arid, maximum net potential NO fluxes are 7600, 63, 270 and 98  $\text{ng m}^{-2} \text{ s}^{-1}$  (in terms of mass of nitric oxide) for cotton, jujube, jujube/cotton mixture and desert soils, respectively.



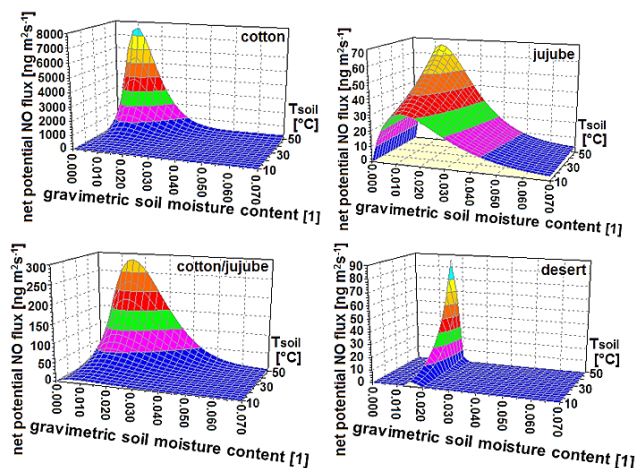


**Figure 2.** Net potential NO fluxes  $F_{\text{NO}}$  ( $\text{ng m}^{-2} \text{s}^{-1}$ ; in terms of mass of nitric oxide) from soils of the four major land-cover types of Milan oasis as functions of soil temperature ( $^{\circ}\text{C}$ ) and dimensionless gravimetric soil moisture content.

### 3.2 Land-cover types of Milan oasis and actual NO fluxes

As mentioned in Section 2.2.5, land-cover classification and actual distribution of Milan oasis' fields have been identified from satellite images (Quickbird, Landsat ETM+). The 2011 distribution of fields and the corresponding land cover is shown in Fig. 3.

The dominant crop was cotton, representing 18 % ( $64 \text{ km}^2$ ) of the total field area of Milan oasis (jujube 7 %,  $28 \text{ km}^2$ ), cotton/jujube mixture 0.89 % ( $3 \text{ km}^2$ ), natural forest 18 % ( $64 \text{ km}^2$ ), residential area 1.62 % ( $5.5 \text{ km}^2$ ) and desert 52 % ( $174 \text{ km}^2$ ). Land-cover specific, actual NO fluxes (30 min means) from cotton, jujube, cotton/jujube and desert soils were calculated from corresponding laboratory-derived net potential NO fluxes, land-type specific soil moisture and soil temperature data (see Sect. 2.2.6). These NO fluxes ( $\text{ng m}^{-2} \text{s}^{-1}$ , in terms of mass of nitric oxide) were then assigned to each individual source unit (i.e. to each of the 2500 polygons of Milan oasis' domain).

For the period 3–24 June 2011, land-cover specific, actual NO fluxes were calculated according to Eq. (10) for cotton, jujube, cotton/jujube and desert soils from corresponding laboratory-derived net potential NO fluxes. As input we used land-type specific, measured soil temperature data as well as land-type specific soil moisture data (so-called “wilting points”, Sect. 2.2.3). The calculated NO fluxes are shown in Fig. 4 as median diel variation (for the entire period of 3–24 June, 2011). Since NO fluxes from Milan cotton fields dominate the total soil biogenic NO emission of the oasis, corresponding medians and quartiles are shown in Fig. 4, while – for the sake of clarity – for jujube, cotton/jujube and desert only medians are given. Since land-type specific “wilting points” are constant, diel variations of actual NO

fluxes mirror directly those of corresponding soil temperatures, showing the daily minimum around 06:00 LT for all four major land-cover types. The maximum of the actual NO-flux, however, is around 13:00 LT for jujube, cotton/jujube and desert soils, and 15:00 LT for cotton. This is due to the growth of the cotton plants: while at the beginning of the experimental period the bare soil surface was nearly 100 % exposed to insolation, the growing cotton canopy has shaded great parts of the soil surface towards the end of the experimental period. This is also reflected by the skewed distribution of actual NO fluxes from cotton-covered soil, indicated by the daytime non-symmetric inter-quartile range (= upper quartile – lower quartile). As shown in Sect. 3.5, actual NO flux data of 09 June, 2011 (08:30–14:30 LT) were used for the comparison of LASAT and MAX-DOAS results. During this particular day (within the first week of the experimental period), the derived flux for “land-cover cotton” ranged from 15–64  $\text{ng m}^{-2} \text{s}^{-1}$  (in terms of mass of NO), those for jujube, cotton/jujube, and desert land covers ranged from 11–13, 6–16, and 6–17  $\text{ng m}^{-2} \text{s}^{-1}$ , respectively. These actual NO fluxes were then assigned to each individual source unit (i.e. to each of the 2500 polygons of Milan oasis' domain). The soil biogenic NO emission from all cotton fields between 08:30 and 14:30 was estimated to be 28.7 kg (in terms of mass of NO), equivalent to 76 % of the total soil biogenic NO emission of the entire Milan oasis within 6 h.

### 3.3 Vertical NO<sub>2</sub> column densities by MAX-DOAS

We performed 32 individual MAX-DOAS measurements within 21 days of the 2011 field campaign to examine the spatial variation between the observed sites. In Fig. 5, all observed vertical NO<sub>2</sub> column densities (in molecules  $\text{cm}^{-2}$ ) observed at sites (1)–(4) of Milan oasis are shown in polar coordinates with reference to corresponding wind directions measured in situ at the individual sites.

Wind speeds (30 min means) ranged between 1.5 and  $7.7 \text{ m s}^{-1}$  and wind direction was mostly (78 %) from the northern quadrants (59, 9, 13 and 19 % from NE, SE, SW and NE quadrants, respectively). As expected, highest VCDs ( $10^{15}$ – $10^{16}$  molecules  $\text{cm}^{-2}$ ) were observed at site (4) (Milan oasis centre), regardless of wind direction. When the wind direction is from the NE quadrant, site (3) (jujube fields) is downwind of Milan oasis (see Fig. 1); then its VCDs are as high as those obtained in the oasis' centre ( $5$ – $7 \times 10^{15}$  molecules  $\text{cm}^{-2}$ ). The few VCD data points of  $1 \times 10^{15}$  molecules  $\text{cm}^{-2}$  at the jujube site, attributed to winds from SE and SW quadrants, are mainly due to NO emissions from traffic on the National Road 315 which passes the southern margins of Milan oasis. Lowest VCDs ( $3 \times 10^{13}$ – $3 \times 10^{14}$  molecules  $\text{cm}^{-2}$ ) have been observed at site (1) (natural forest) and site (2) (desert). Alone from these spatially resolved VCD observations in the Milan oasis' domain, the increase of VCD due to the oasis itself can be estimated to be of at least one order of magnitude.

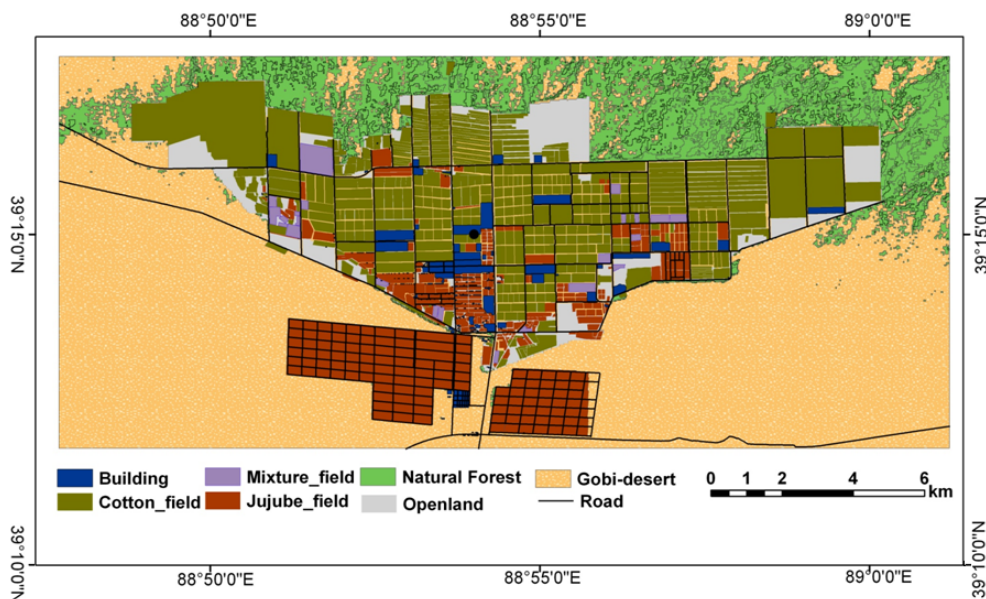


**Figure 3.** 2011 map of land-cover types of Milan oasis as derived from satellite images (Quickbird, Landsat ETM+, see Sect. 2.2.5).

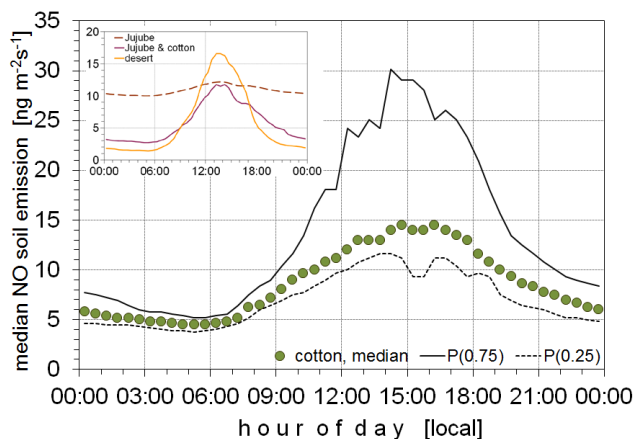


**Figure 4.** Median diel variation of the actual NO-flux ( $\text{ng m}^{-2} \text{s}^{-1}$ ; in terms of mass of nitric oxide) from soils of the four major land-cover types of Milan oasis for the period 3–24 June, 2011. Data have been calculated according Eq. (10) using (a) soil temperatures (medians) measured for each of the four major land-cover types, and (b) so-called “wilting point” data for corresponding soil moisture contents at the four sites (see Sect. 2.2.3). Data for the cotton site are given as medians, as well as 25 and 75 % quantiles, and those for the Jujube, Jujube-cotton and desert sites as medians only (see figure insert).

Fortunately, we were able to perform simultaneous measurements with two MAX-DOAS instruments at sites (1) and (3) on 09 and 13 June, 2011. Since winds (approx.  $3 \text{ m s}^{-1}$ ) were from the NE quadrant on these days, site (1) was upwind, and site (3) downwind of Milan oasis. Corresponding VCD results are shown in Fig. 6. NO<sub>2</sub> VCDs at the down-

wind site exceeded those at the upwind site by a factor of 5–9. This difference between downwind and upwind MAX-DOAS signals is considered to be a direct measure for the areal increase of ambient NO<sub>2</sub> concentration. In the absence of anthropogenic NO<sub>x</sub> sources (see Sect. 2.1), this provides first evidence for the considerable impact of the biogenic NO emissions from the fields of Milan oasis.

### 3.4 3-D distribution of ambient NO-concentration

The LASAT model has to be used to calculate the dispersion of soil emitted NO into the atmospheric boundary layer over Milan oasis. An example for the resulting distribution of NO concentration in the first four vertical layers of LASAT (0–3, 3–5, 5–10 and 10–20 m) is shown in Fig. 7 (9 June, 2011; 11:30–13:00 LT). The shown results are the mean of three LASAT model runs, since a new LASAT calculation of 3-D distribution of NO concentration is started for every set of meteorological parameters which are provided every 30 min from means of the in situ measured meteorological quantities (see Sect. 2.2.2). During 11:30–13:00, mean wind direction was 15, 38 and 50°, wind speed was rather constant ( $2.60\text{--}2.67 \text{ m s}^{-1}$ ) and atmospheric stability class was generally neutral (3.2).

By comparing the NO ambient concentrations, particularly in the first vertical LASAT layer (0–3 m) of oasis area with the surrounding desert, it becomes obvious that the great differences of ambient NO concentrations mirror the corresponding differences of actual soil NO fluxes from each source unit; within this layer calculated mean NO concentrations are 13, 12, 10 and  $1 \text{ ng m}^{-3}$  (in terms of mass of nitric oxide; or 10.6, 9.8, 8.2 and 0.8 ppb) for the oasis cen-

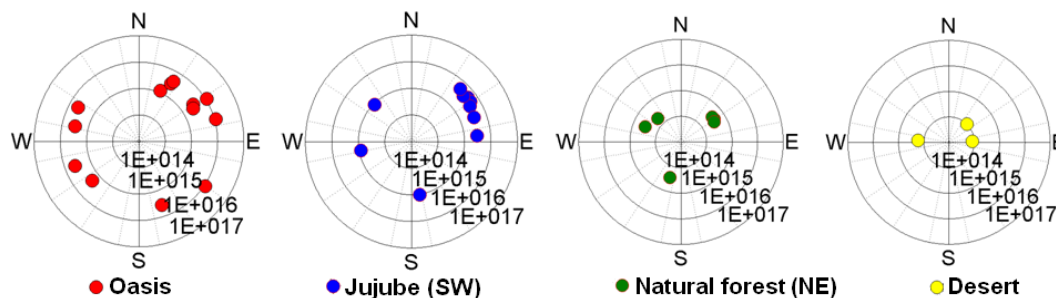


**Figure 5.** Results of MAX-DOAS measurements performed at sites oasis/hotel (4), jujube (4), natural forest (1) and desert (2) of Milan oasis from 23 May to 26 June, 2011 (see Fig. 1). Vertical NO<sub>2</sub> column densities (in molecules cm<sup>-2</sup>; 20–30 min averages) are shown in relation to in situ measured wind direction at each location of MAX-DOAS measurements. The MAX-DOAS measurements were performed between 06:00 and 19:00 LT. Note the radial logarithmic scale of VCD data.

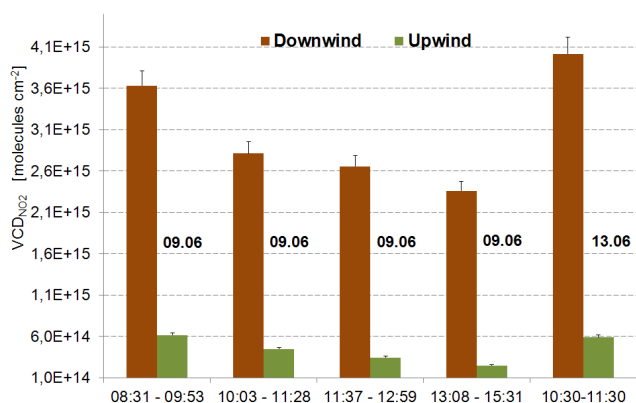


**Figure 6.** Results of NO<sub>2</sub> VCD measured simultaneously with two MAX-DOAS instruments upwind (natural forest, site (1)) and downwind (jujube field, site (3)) of Milan oasis on 9 and 13 June, 2011.

tre, jujube fields, cotton/jujube mixture and desert, respectively. The value at the oasis centre exceeds those over desert by more than an order of magnitude, similar to the corresponding VCD values (see above). As expected under the prevailing conditions of well-developed atmospheric turbulence, NO concentration rapidly decreases with height (see panels “0–3 m”, “3–5 m”, “5–10 m” in Fig. 7), and with prevailing northerly winds, the NO concentration centre shifting southwards with increasing altitude.

### 3.5 Simulated SCDs and VCDs vs. SCDs and VCDs by MAX-DOAS

For those periods where simultaneous “upwind” and “downwind” MAX-DOAS measurements have been performed (9 and 13 June, 2011), corresponding SCD<sub>sim</sub> and VCD<sub>sim</sub> have been simulated by suitable vertical integration (see Sect. 2.2.8) of LASAT-calculated 3-D NO concentrations, followed by NO→NO<sub>2</sub> conversion (based on photostationary state assumption of Milan oasis’ atmospheric boundary

layer). Since SCD<sub>sim</sub> and VCD<sub>sim</sub> represent only that part of true SCDs and VCDs of NO<sub>2</sub>, which are due to the contribution of the oasis’ soil NO emissions, SCD<sub>sim</sub> and VCD<sub>sim</sub> are compared to the difference of those SCDs and VCDs which have been simultaneously measured by two MAX-DOAS instruments at corresponding “downwind” and “upwind” sites (see Fig. 8). For elevation angles of 2 and 4°, SCD<sub>sim</sub> and ΔSCD = SCD<sub>down</sub> – SCD<sub>up</sub> are shown in Fig. 8a. In Fig. 8b, VCD<sub>sim</sub> and ΔVCD = VCD<sub>down</sub> – VCD<sub>up</sub> are shown for 15° elevation.

Here it should be noted that in principle the accuracy of the geometric approximation is higher for the high-elevation angles than for the lower-elevation angles. However, for the specific cases studied here, this is not the case. First, close to the sources, the height of the layer with elevated NO<sub>2</sub> is quite low (in our case the bulk of NO<sub>2</sub> is located below 100 m). Second, also the aerosol load is usually very low. Thus the probability of scattering events inside the layer of enhanced NO<sub>2</sub> is very low, and consequently the accuracy of the geometric approximation is relatively high. To further quantify the associated uncertainties, we performed radiative transfer simulations and found that the deviations from the geometric approximation are similar for the different elevation angles (about 5 % for 2°, 3 % for 4° and 3 % for 15°). However, because of the shorter light paths through the NO<sub>2</sub> layer, the relative error caused by the uncertainty of the spectral analysis is higher than for the low-elevation angles. Thus for the case of our measurements, we indeed expect lower uncertainties for the low-elevation angles.

Since soil NO emission data used in the LASAT dispersion model were calculated from land-cover type specific potential net NO fluxes, which in turn were derived from laboratory incubation experiments on corresponding soil samples, the results in Fig. 8 are also considered as an excellent quality assurance of the chosen up-scaling of laboratory results to the oasis scale. There is remarkably good agreement between measured and simulated data.

However, the actual NO emissions (irrespective of the land-cover type) have their maximum in the early afternoon

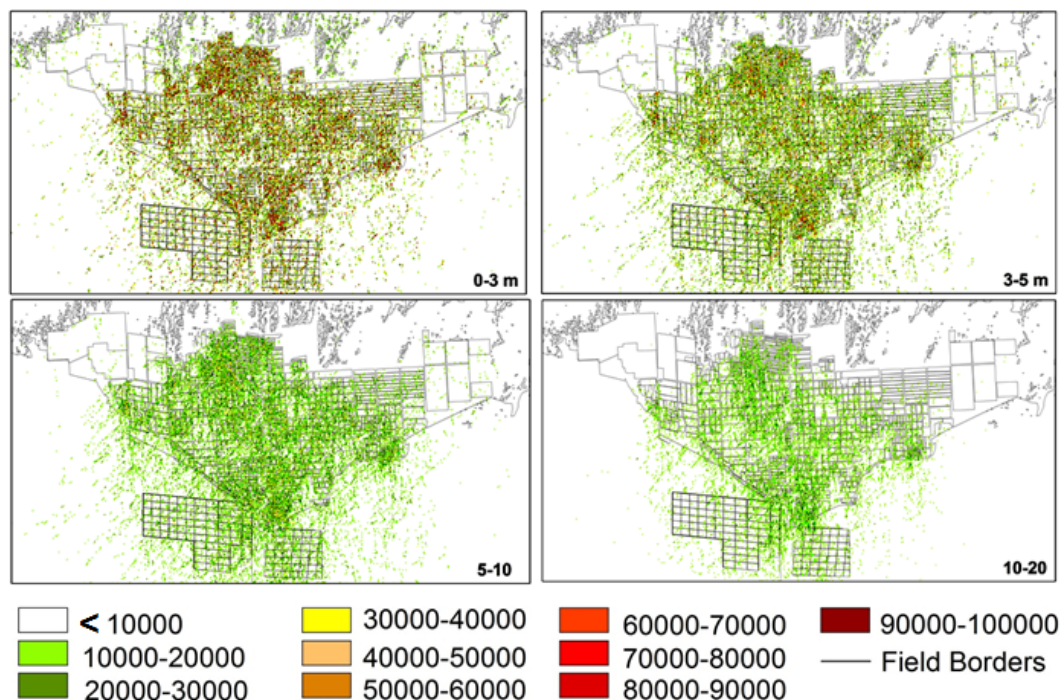


**Figure 7.** Results of NO concentrations ( $\text{ng m}^{-3}$ ; in terms of mass of nitric oxide) calculated by the LASAT dispersion model for the first four vertical levels on 9 June, 2011, 11:30 to 13:00 LT.

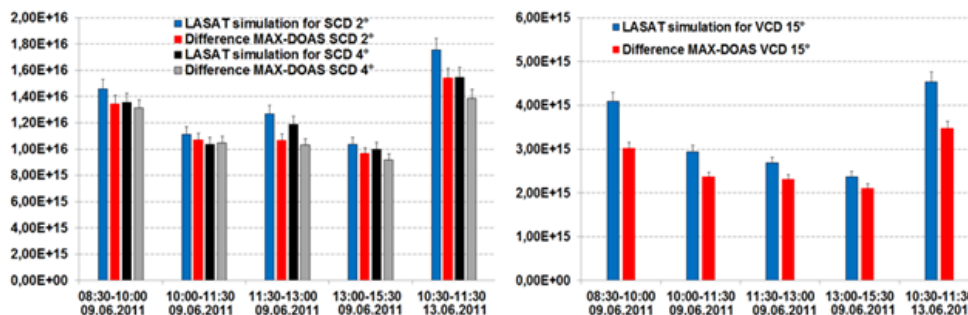
(see Fig. 4), while the highest height-integrated NO<sub>2</sub> concentrations as simulated by LASAT (on the basis of the actual NO emissions) are in the morning (08:30–10:00), followed by rather constant values for the remainder of the day (see Fig. 8). The apparent discrepancy between both diurnal variations can be simply explained by the diurnal variation of the wind direction and the specific viewing geometry of the MAX-DOAS instrument. The MAX-DOAS instrument was located at the southwest corner of the oasis, and the observations at zenith and low elevation angles probed air masses located at different locations across the oasis. The wind direction was from northeast in the morning and turned to northwest in the afternoon. Hence, air masses of lower concentration crossed the viewing directions in the afternoon compared to those in the morning. This explains why, in spite of the larger NO<sub>x</sub> emissions, smaller column densities were observed in the afternoon. The apparent discrepancy of the diurnal cycles of NO emissions and measured NO<sub>2</sub> column densities indicates the importance of exactly considering the 3-D NO<sub>2</sub> distribution (due to the soil-emitted NO) for the comparison of the model results with MAX-DOAS observations.

Figure 8b shows that the LASAT simulations overestimate slightly the true NO<sub>2</sub> VCD. Both measured and simulated NO<sub>2</sub> VSDs have an average root mean square error between the measured and simulated values of approx. 5–15%. However, the overestimation of LASAT simulation is well suited

to the fact that in reality a little less NO can be converted to the NO<sub>2</sub> because of lower ozone concentration at the surface.

#### 4 Conclusions

This study has been focused on the following activities: (1) representative soil sampling from the uppermost soil layer ( $<0.05$  m) of all land-cover type units (natural forest, cotton fields, jujube fields, cotton/jujube mixture, desert) of Milan oasis (Xinjiang, NW China), (2) laboratory incubation experiments (dynamic chamber system) to characterize the biogenic NO emission from these soil samples in the form of net potential NO fluxes as function of soil moisture and soil temperature, (3) determination of the actual size, areal distribution and land-cover type of Milan oasis' field units from satellite remote sensing information, (4) field measurements of slant (SCD) and vertical (VCD) NO<sub>2</sub> column densities (by MAX-DOAS) and additional quantities (soil moisture, soil temperature, ozone concentration, NO<sub>2</sub> photolysis rate, meteorological parameters) during an extended field campaign of 4 weeks at Milan oasis, (5) using data from (2), (3) and (4): calculation of Milan oasis' 2-D distribution of actual land-cover specific NO fluxes, (6) calculation of 3-D NO concentrations in Milan oasis' atmospheric boundary layer originating from the dispersion of biogenic NO soil emissions determined by (5) with help of the Lagrangian dispersion model LASAT, (7) simulation of SCDs and VCDs by



**Figure 8.** Simulated SCDs vs. SCDs measured by MAX-DOAS (a) and simulated VCDs vs. VCDs measured by MAX-DOAS (b) on 9 and 13 June, 2011 at Milan oasis. SCDs were measured and simulated for elevation angles of 2 and 4°; VCDs were measured at 15°.

suitable vertical integration of calculated 3-D NO concentrations followed by suitable NO $\rightarrow$ NO<sub>2</sub> conversion factors derived from in situ measurements, and (8) comparison of measured and simulated SCDs and VCDs.

Results of the laboratory-derived NO fluxes have shown that the extensively managed (fertilized and efficiently irrigated) cotton fields of Milan oasis release large amounts of soil biogenic NO; NO fluxes range between 10–30 ng m<sup>-2</sup> s<sup>-1</sup> (in terms of mass of N), which is approx. 5–10 times more than from a typical central European wheat field (Yamulki et al., 1995; Stohl et al., 1996).

Applying two MAX-DOAS instruments, simultaneous measurements were performed at upwind and downwind sites of Milan oasis. Downwind site VCDs exceeded those from the upwind site by factors of 5–9. Differences of VCD and SSC (“downwind” minus “upwind”) are a direct measure for the areal increase of ambient NO<sub>2</sub> concentration caused by the oasis itself. The measured differences of VCDs and SCDs were compared with the simulated VCDs and SCDs and excellent agreement was found.

This agreement is considered as the first successful attempt to prove the validity of the chosen approach to upscale laboratory-derived biogenic NO fluxes to ecosystem level field conditions, i.e. from the spatial scale of a soil sample (cm<sup>2</sup>) to field size (ha), and from field size (ha) to the size of an entire (agro-)ecosystem (km<sup>2</sup>). Furthermore, in the absence of anthropogenic NO sources of Milan oasis (hydropower energy, battery powered trikes), it is obvious that the areal increase of ambient NO<sub>2</sub> concentration in the atmospheric boundary layer of the isolated (in terms of NO<sub>2</sub> advection) Milan oasis is entirely due to biogenic NO emission from the arid/hyper-arid soils of the oasis itself. Extensive agricultural management of Milan oasis’ crop fields (fertilization (350–600 kg N ha<sup>-1</sup> a<sup>-1</sup>) and effective irrigation of cotton and jujube fields) obviously provides considerable contribution of biogenic NO<sub>x</sub> (NO + NO<sub>2</sub>) from arid/hyper-arid soils of the Taklimakan desert to the local tropospheric NO<sub>x</sub> budget.

About 80 % of the Chinese cotton production originates from the 3000 km long belt of oases surrounding Taklimakan Desert (1.65 × 10<sup>6</sup> km<sup>2</sup>) in Xinjiang (NW China); cotton cultivated land area in Xinjiang occupies top rank in all of China. Since 1955, Xinjiang’s output of cotton has increased by a factor of 294 (Lei et al., 2005). Fast economic growth in the region (+11 % GDP a<sup>-1</sup>), inevitably accompanied by large anthropogenic NO<sub>x</sub> emissions (traffic, energy production), may be countervailed or even exceeded by the “hotspot” character of Xinjiang’s oases, namely by soil biogenic NO emissions from agriculturally dominated oases. Most likely, they will contribute most to the regional tropospheric NO<sub>x</sub> budget. This is all the more likely, given the continued intensification of oasis agriculture around the Taklimakan desert which will be accompanied by corresponding land use change (desert $\rightarrow$ dryland farming with irrigation) in the coming decades.

*Acknowledgements.* This work was funded through the German Research Foundation (DFG) project “DEQNO – Desert Encroachment in Central Asia – Quantification of soil biogenic Nitric Oxide” (DFG-MA 4798/1-1), the Max Planck Society (MPG), and the Max Planck Graduate Centre with Johannes Gutenberg-University Mainz (MPGC). The authors like to thank Guozheng Song, Günter Schebeske, Achim Zipka, Yanhong Li, Fanxia Wang, Aixia Yang, Sijun Luo and Zhilin Zhu for their field assistance and their substantial support before, during and after the DEQNO 2011 campaign. We also thank Reza Shaiganfar and Steffen Beirle for their support during pre-preparation of the MAX-DOAS instrument.

The service charges for this open access publication have been covered by the Max Planck Society.

Edited by: P. Jöckel

## References

- Ashuri, F. A.: Der Austausch von Stickstoffmonoxid zwischen Boden und Atmosphäre unter besonderer Berücksichtigung des Bodenwassergehaltes, Einfluss kulturlandschaftlicher Verhältnisse auf den Umsatz eines Spurengases. Ph.D. thesis, Johannes Gutenberg University Mainz, Mainz, Germany, 1–169, 2009.
- Atkinson, R., Baulch, D. L., Cox, R. A., Crowley, J. N., Hampson, R. F., Hynes, R. G., Jenkin, M. E., Rossi, M. J., and Troe, J.: Evaluated kinetic and photochemical data for atmospheric chemistry: Volume I – gas phase reactions of O<sub>x</sub>, HO<sub>x</sub>, NO<sub>x</sub> and SO<sub>x</sub> species, *Atmos. Chem. Phys.*, 4, 1461–1738, doi:10.5194/acp-4-1461-2004, 2004.
- Bargsten, A., Falge, E., Pritsch, K., Huwe, B., and Meixner, F. X.: Laboratory measurements of nitric oxide release from forest soil with a thick organic layer under different understory types, *Biogeosciences*, 7, 1425–1441, doi:10.5194/bg-7-1425-2010, 2010.
- Behrendt, T., Veres, P. R., Ashuri, F., Song, G., Flanz, M., Mamtimin, B., Bruse, M., Williams, J., and Meixner, F. X.: Characterisation of NO production and consumption: new insights by an improved laboratory dynamic chamber technique, *Biogeosciences Discuss.*, 11, 1187–1275, doi:10.5194/bgd-11-1187-2014, 2014.
- Beirle, S., Platt, U., Wenig, M., and Wagner, T.: Highly resolved global distribution of tropospheric NO<sub>2</sub> using GOME narrow swath mode data, *Atmos. Chem. Phys.*, 4, 1913–1924, doi:10.5194/acp-4-1913-2004, 2004.
- Bogumil, K., Orphal, J., Homann, T., Voigt, S., Spietz, P., Fleischmann, O. C., Vogel, A., Hartmann, A., Kromminga, H., Bovensmann, H., Frerick, J., and Burrows, J. P.: Measurements of molecular absorption spectra with the SCIAMACHY pre-flight model: instrument characterization and reference data for atmospheric remote-sensing in the 230–2380 nm region, *J. Photoch. Photobiol. A*, 157, 167–184, 2003.
- Brinksmas, E. J., Pinardi, G., Volten, H., Braak, R., Richter, A., Schoenhardt, A., Van Roozendaal, M., Fayt, C., Hermans, C., Dirksen, R. J., Vlemmix, T., Berkhout, A. J. C., Swart, D. P. J., Oetjen, H., Wittrock, F., Wagner, T., Ibrahim, O. W., Leeuw, G. de., Moerman, M., Curier, R. L., Celarier, E. A., Cede, A., Knap, W. H., Veefkind, J. P., Eskes, H. J., Allaart, M., Rothe, R., Pitters, A. J. M., and Levelt, P. F.: The 2005 and 2006 DANDELIONS NO<sub>2</sub> and aerosol intercomparison campaigns, *J. Geophys. Res.*, 113, 1–18, 2008.
- Chameides, W. L., Fehsenfeld, F., Rodgers, M. O., Cardelino, C., Martinez, J., Parrish, D., Lonneman, W., Lawson, D. R., Rasmussen, R. A., Zimmerman, P., Greenberg, J., Middleton, P., and Wang, T.: Ozone precursor relationships in the ambient atmosphere, *J. Geophys. Res.*, 92, 6037–6055, 1992.
- Chander, G. and Markham, B.: Revised Landsat-5 TM radiometric calibration procedures and postcalibration dynamic ranges, *IEEE T. Geosci. Remote*, 41, 2674–2677, 2003.
- Conrad, R.: Soil Microorganisms as controllers of atmospheric trace gases (H<sub>2</sub>, CO, CH<sub>4</sub>, COS, N<sub>2</sub>O and NO), *Microbiol. Rev.*, 60, 609–640, 1996.
- Crutzen, P. J.: Role of the tropics in atmospheric chemistry, in: *The Geophysiology of Amazonia*, edited by: Dickinson, R. E., John Wiley & Sons, New York, 107–132, 1987.
- Davidson, E. A. and Kinglerlee, W.: A global inventory of nitric oxide emissions from soils, *Nutr. Cycl. Agroecosys.*, 48, 37–50, 1997.
- Denman, K. L., Brasseur, G. P., Chidthaisong, A., Ciais, P., Cox, P. M., Dickinson, R. E., Hauglustaine, D., Heinze, C., Holland, E. A., Jacob, D. J., Lohmann, U., Ramachandran, S., Da Silva Dias, P. L., Wofsy, S. C., and Zhang, X.: Couplings between changes in the climate system and biogeochemistry, in *Climate Change 2007: The physical science basis. Contribution of working group 1 to the fourth assessment report of the Intergovernmental Panel on Climate Change*, edited by: Solomon, S., Qin, D., Manning, M., Chen, Z., Marquis, M., Averyt, K. B., Tignor, M., Miller, H. L., Cambridge University Press, Cambridge, 499–588, 2007.
- Feig, G. T.: Soil Biogenic Emissions of Nitric Oxide from Arid and Semi-Arid Ecosystems, Ph.D. thesis, Johannes Gutenberg University Mainz, Mainz, Germany, 1–222, 2009.
- Feig, G. T., Mamtimin, B., and Meixner, F. X.: Soil biogenic emissions of nitric oxide from a semi-arid savanna in South Africa, *Biogeosciences*, 5, 1723–1738, doi:10.5194/bg-5-1723-2008, 2008a.
- Feig, G. T., Mamtimin, B., and Meixner, F. X.: Use of laboratory and remote sensing techniques to estimate vegetation patch scale emissions of nitric oxide from an arid Kalahari savanna, *Biogeosciences Discuss.*, 5, 4621–4680, doi:10.5194/bgd-5-4621-2008, 2008b.
- Galbally, I. E. and Johansson, C.: A model relating laboratory measurements of rates of nitric oxide production and field measurements of nitric oxide emissions from soils, *J. Geophys. Res.*, 94, 6473–6480, 1989.
- Ganzeveld, L., Eerdeken, G., Feig, G., Fischer, H., Harder, H., Königstedt, R., Kubistin, D., Martinez, M., Meixner, F. X., Scheeren, H. A., Sinha, V., Taraborrelli, D., Williams, J., Vilà-Guerau de Arellano, J., and Lelieveld, J.: Surface and boundary layer exchanges of volatile organic compounds, nitrogen oxides and ozone during the GABRIEL campaign, *Atmos. Chem. Phys.*, 8, 6223–6243, doi:10.5194/acp-8-6223-2008, 2008.
- Gelfand, I., Feig, G., Meixner, F. X., and Yakir, D.: Afforestation of semi-arid shrubland reduces biogenic NO emission from soil, *Soil Biol. Biochem.*, 41, 1561–1570, 2009.
- Harrison, P. and Pearce, F.: *Deserts and Drylands*, AAAS Atlas of Population and Environment, University of California Press, Berkeley, USA, 131–134, 2000.
- Hartge, H. and Horn, R.: *Die physikalische Untersuchung von Böden: Praxis Messmethoden Auswertung*, Schweizerbart'sche Verlagsbuchhandlung, Stuttgart, Germany, 1–178, 2009.
- Hermans, C., Vandeale, A. C., Carleer, M., Fally, S., Colin, R., Jenouvrier, A., Coquart, B., and Merienne, M. F.: Absorption Cross-Sections of Atmospheric Constituents, NO<sub>2</sub>, O<sub>2</sub>, and H<sub>2</sub>O, *Environ. Sci. Pollut. Res.*, 6, 151–158, 1999.
- Hönninger, G. and Platt, U.: The Role of BrO and its Vertical Distribution during Surface Ozone Depletion at Alert, *Atmos. Environ.*, 36, 2481–2489, 2002.
- Hönninger, G., von Friedeburg, C., and Platt, U.: Multi axis differential optical absorption spectroscopy (MAX-DOAS), *Atmos. Chem. Phys.*, 4, 231–254, doi:10.5194/acp-4-231-2004, 2004.
- Husar, R. B., Patterson, D. E., Husar, J. D., Gillani, N. V., and Wilson Jr., W. E.: Sulfur budget of a power plant plume, *Atmos. Environ.*, 12, 549–568, doi:10.1016/0004-6981(78)90236-6, 1978.
- IVU Umwelt GmbH: LASarc – GIS integration of LASAT, Environmental Planning and Information Systems, Freiburg, Germany, 2012.

- Janicke Consulting: Dispersion model LASAT, Version 3.2, Reference Book, Janicke Consulting, Überlingen, Germany, 239 pp., 2011.
- Kargas, G., Ntoulas, N., and Nektarios, P. A.: Soil texture and salinity effects on calibration of TDR300 dielectric moisture sensor, *Soil Research*, 51, 330–340, 2013.
- Kirkman, G. A., Yang, W. X., and Meixner, F. X.: Biogenic nitric oxide emissions upscaling: an approach for Zimbabwe, *Global Biogeochem. Cy.*, 15, 1005–1020, 2001.
- Köppen, W.: *Grundriss der Klimakunde*, Gruyter Verlag, Berlin/Leipzig, Germany, 388 pp., 1931.
- Kottek, M., Grieser, J., Beck, C., Rudolf, B., and Rubel, F.: World Map of the Köppen-Geiger climate classification Updated, *Meteorologische Zeitschrift*, 15, 259–263, 2006.
- Kurucz, R. L., Furenli, I., Brault, J., and Testerman, L.: Solar Flux Atlas from 296 nm to 1300 nm, National Solar Observatory Atlas No. 1 Office of University publisher, Harvard University, Cambridge, 1984.
- Lei, J. and Zhang, X. L.: Structural adjustment of oasis agriculture in Xinjiang, *Chinese Journal of Population, Resources and Environment*, 3, 29–33, 2005.
- Leighton, P. A.: *Photochemistry of Air Pollution*, Academic Press, New York and London, 300 pp., 1961.
- Leue, C., Wenig, M., Wagner, T., Platt, U., and Jähne, B.: Quantitative analysis of NO<sub>x</sub> emissions from GOME satellite image sequences, *J. Geophys. Res.*, 106, 5493–5505, 2001.
- Ludwig, J., Meixner, F. X., Vogel, B., and Förstner, J.: Processes, influencing factors, and modelling of nitric oxide surface exchange – an overview, *Biogeochemistry*, 52, 225–257, 2001.
- Mayer, J.-C., Bargsten, A., Rummel, U., Meixner, F. X., and Foken, T.: Distributed modified bowen ratio method for surface layer fluxes of reactive and non-reactive trace gases, *Agr. Forest Meteorol.*, 151, 655–668, 2011.
- Meixner, F. X., Ajavon, A.-L., Helas, G., Scharffe, D., Zenker, T., Harris, G. W., and Andreae, M. O.: Vertical distribution of ozone over southern Africa: Airborne measurements during SAFARI-92, AGU Fall Meeting, San Francisco, U.S.A., 1993.
- Meixner, F. X. and Yang, W. X.: Biogenic emissions of nitric oxide and nitrous oxide from arid and semiarid land, in: *Dryland Ecohydrology*, edited by: D'Odorico, P. and Porporat, A., Springer, Dordrecht, the Netherlands, 233t255, 2006, 233–255, 2006.
- Morse, A., Tasumi, M., Allen, R. G., and Kramber, W. J.: Application of the SEBAL Methodology for Estimating Consumptive Use of Water and Streamflow Depletion in the Bear River Basin of Idaho through Remote Sensing. Final report submitted to The Raytheon Systems Company, Earth Observation System Data and Information System Project, Boise, USA, 107 pp., 2000.
- Otter, L. B., Yang, W. X., Scholes, M. C., and Meixner, F. X.: Nitric oxide emissions from a southern African Savannah, *J. Geophys. Res.*, 104, 18471–18485, 1999.
- Perumal, K. and Bhaskaran, R.: Supervised classification performance of multispectral images, *Journal of Computing*, 2–2, 124–129, 2010.
- Platt, U. and Stutz, J.: *Differential Optical Absorption Spectroscopy: Principles and Applications*, Springer, Berlin, Heidelberg, Germany, 135–377, 2008.
- Rothman, L. S., Jacquemart, D., Barbe, A., Chris Benner, D., Birk, M., Brown, L. R., Carleer, M. R., Chackerian Jr, C., Chance, K., Coudert, L. H., Dana, V., Devi, V. M., Flaud, J.-M., Gamache, R. R., Goldman, A., Hartmann, J.-H., Jucks, K. W., Maki, A. G., Mandin, J.-Y., Massie, S. T., Orphal, J., Perrin, A., Rinsland, C. P., Smith, M. A. H., Tennyson, J., Tolchenov, R. N., Toth, R. A., Vander Auwera, J., Varanasi, P., and Wagner, G.: The HITRAN 2004 molecular spectroscopic database, *J. Quant. Spectrosc. Ra.*, 96, 139–204, 2005.
- Rudolph, J. and Conrad, R.: Flux between soil and atmosphere, vertical concentration profiles in soil, and turnover of nitric oxide: 2. Experiments with naturally layered soil cores, *J. Atmos. Chem.*, 23, 275–300, 1996.
- Rudolph, J., Rothfuss, F., and Conrad, R.: Flux between soil and atmosphere, vertical concentration profiles in soil, and turnover of nitric oxide: 1. Measurements on a model soil core, *J. Atmos. Chem.*, 23, 253–273, 1996.
- Richter, A. and Burrows, J. P.: Tropospheric NO<sub>2</sub> from GOME Measurements, *Adv. Space Res.*, 29, 1673–1683, 2002.
- Simiu, E. and Scanlan, R. H.: *Wind Effects on Structures: Fundamentals and Applications to Design*, 3rd edn., John Wiley & Sons, New York, USA, 704 pp., 1996.
- Sinreich, R., Frieß, U., Wagner, T., and Platt, U.: Multi axis differential optical absorption spectroscopy (MAX-DOAS) of gas and aerosol distributions, *Faraday Discuss.*, 130, 153–164, doi:10.1039/b419274p, 2005.
- Solomon, S., Schmeltekopf, A. L., and Sanders, R. W.: On the interpretation of zenith sky absorption measurements, *J. Geophys. Res.*, 92, 8311–8319, doi:10.1029/JD092iD07p08311, 1987.
- Stohl, A., Williams, E., Wotawa, G., and Kolb, H. K.: A European Inventory of Soil Nitric Oxide Emissions and the Effect of these Emissions on the Photochemical Formation of Ozone, *Atmos. Environ.*, 30, 3741–3755, 1996.
- Stull, R. B.: *An Introduction to Boundary-Layer Meteorology*, Kluwer Academic Publishers, Dordrecht, The Netherlands, 671 pp., 1988.
- Trebs, I., Bohn, B., Ammann, C., Rummel, U., Blumthaler, M., Königstedt, R., Meixner, F. X., Fan, S., and Andreae, M. O.: Relationship between the NO<sub>2</sub> photolysis frequency and the solar global irradiance, *Atmos. Meas. Tech.*, 2, 725–739, doi:10.5194/amt-2-725-2009, 2009.
- Turner, D. B.: *Workbook of Atmospheric Dispersion Estimates*, 2nd edn., Lewis publisher, London, 175 pp., 1994.
- van Dijk, S. and Meixner, F. X.: Production and consumption of NO in forest and pasture soils from the amazon basin, *Water Air Pollut.-Focus*, 1, 119–130, 2001.
- van Dijk, S. M., Gut, A., Kirkman, G. A., Meixner, F. X., Andreae, M. O., and Gomes, B. M.: Biogenic NO emissions from forest and pasture soils: relating laboratory studies to field measurements, *J. Geophys. Res.*, 107, LBA 25-1–LBA 25-11, doi:10.1029/2001JD000358, 2002.
- Vandaele, A. C., Hermans, C., Simon, P. C., Rozendael, M., Carleer, J. M., and Colin, R.: Fourier transform measurement of NO<sub>2</sub> absorption cross-section in the visible range at room temperature, *J. Atmos. Chem.*, 25, 289–305, 1996.
- Volkamer, R., Spietz, P., Burrows, J., and Platt, U.: High-resolution absorption cross-sections of glyoxal in the UV-vis and IR spectral ranges, *J. Photoch. Photobio. A*, 172, 35–46, 2005.
- Wagner, T., Ibrahim, O., Shaiganfar, R., and Platt, U.: Mobile MAX-DOAS observations of tropospheric trace gases, *Atmos. Meas. Tech.*, 3, 129–140, doi:10.5194/amt-3-129-2010, 2010.

- Wagner, T., Beirle, S., Brauers, T., Deutschmann, T., Friß, U., Hak, C., Halla, J. D., Heue, K. P., Junkermann, W., Li, X., Platt, U., and Pundt-Gruber, I.: Inversion of tropospheric profiles of aerosol extinction and HCHO and NO<sub>2</sub> mixing ratios from MAX-DOAS observations in Milano during the summer of 2003 and comparison with independent data sets, *Atmos. Meas. Tech.*, 4, 2685–2715, doi:10.5194/amt-4-2685-2011, 2011.
- Wittrock, F., Oetjen, H., Richter, A., Fietkau, S., Medeke, T., Rozanov, A., and Burrows, J. P.: MAX-DOAS measurements of atmospheric trace gases in Ny-Ålesund – Radiative transfer studies and their application, *Atmos. Chem. Phys.*, 4, 955–966, doi:10.5194/acp-4-955-2004, 2004.
- Yang, W. X. and Meixner, F. X.: Laboratory studies on the release of nitric oxide from subtropical grassland soils: the effect of soil temperature and moisture, in: *Gaseous Nitrogen Emissions from Grasslands*, Wallingford, England, 67–70, 1997.
- Yamulki, S., Goulding, K. W. T., Webster, C. P., and Harrison, R. M.: Studies on NO and N<sub>2</sub>O Fluxes from a Wheat Field, *Atmos. Environ.*, 29, 1627–1635, doi:10.1016/1352-2310(95)00059-8, 1995.
- Yu, J., Meixner, F. X., Sun, W., Liang, Z., Chen, Y., Mamtimin, B., Wang, G., and Sun, Z.: Biogenic nitric oxide emission from saline sodic soils in a semiarid region, northeastern China: a laboratory study, *J. Geophys. Res.*, 113, 1–11, 2008.
- Yu, J., Meixner, F. X., Sun, W., Mamtimin, B., Wang, G., Qi, X., Xia, C., and Xie, W.: Nitric oxide emissions from black soil, northeastern China: a laboratory study revealing significantly lower rates than hitherto reported, *Soil Biol. Biochem.*, 42, 1784–1792, 2010a.
- Yu, J., Meixner, F. X., Sun, W., Mamtimin, B., Xia, C., and Xie, W.: Biogenic nitric oxide emission of mountain soils sampled from different vertical landscape zones in the Changbai Mountains, Northeastern China, *Environ. Sci. Technol.*, 44, 4122–4128, 2010b.